Experiments in Fluids 23 (1997) 361–372

Molecular tagging velocimetry and other novel applications of a new phosphorescent supramolecule

C. P. Gendrich, M. M. Koochesfahani, D. G. Nocera

Abstract The development and applications of a new class of water-soluble compounds suitable for molecular tagging diagnostics are described. These molecular complexes are formed by mixing a lumophore, an appropriate alcohol, and cyclodextrin. Using 1-BrNp as the lumophore, cyclohexanol is determined to be the most effective overall among the alcohols for which data are currently available. Information is provided for the design of experiments based on these complexes along with a less complex method for generating the grid patterns typically used for velocimetry. Implementation of a two-detector system is described which, in combination with a spatial correlation technique for determining velocities, relaxes the requirement that the initial tagging pattern be known *a priori*, eliminates errors in velocity estimates caused by variations in the grid pattern during an experiment, and makes it possible to study flows with non-uniform mixtures. This detection and analysis combination also solves one of the problems associated with using caged fluorescein to study high-speed flows. In addition to the traditional implementation for velocimetry, novel applications for studying the Lagrangian evolution of both reacting and non-reacting interfaces and obtaining combined passive scalar/velocity measurements are demonstrated.

Received: *26 August 1996*/*Accepted*: *13 March 1997*

C. P. Gendrich, M. M. Koochesfahani
Department of Mechanical Engineering
Michigan State University
E. Lansing, Mi 48824, USA

D. G. Nocera
Department of Chemistry
Massachusetts Institute of Technology
Cambridge, MA 02139, USA

Correspondence to: C. P. Gendrich

This work was supported in part by the Air Force Office of Scientific Research under grants F49620-92-J-0338 and F49620-95-1-0391, and by the MRSEC Program of the National Science Foundation under award DMR-9400417.

The supramolecular systems described in this work were developed in house. Inquiries regarding further information on these chemicals and their availability should be addressed to D. G. Nocera or M. M. Koochesfahani.

1 Introduction

Past efforts in the use of molecular tagging diagnostics for flow studies have traditionally concentrated on velocimetry. A variety of molecules have been utilized for this purpose, and regardless of the detailed photophysics of each, their use can collectively be discussed under a common heading of Molecular Tagging Velocimetry (MTV). In this method, the flowing medium is premixed uniformly with molecules that can be turned into long-lifetime tracers upon excitation by photons of an appropriate wavelength. Typically a pulsed laser is used to "tag" the regions of interest, and those tagged regions are interrogated at two successive times within the lifetime of the tracer. The measured displacement vector provides the estimate of the velocity vector.

A molecular complex is suitable for molecular tagging applications if its lifetime as a tracer is long enough relative to the flow convection time scale to allow sufficient displacement of the tagged regions. MTV investigations in liquid-phase flows have, until recently, relied on photochromic molecules, which has required experimentalists to use organic solvents such as kerosene as the flowing medium (Popovich and Hummel 1967; Falco and Chu 1987; Ojha et al. 1989; Chu and Liao 1992; Chu et al. 1993; among others). In a photochromic process excitation by photons causes a change in the absorption spectrum and therefore a change in the color of the solution (e.g. from clear to dark blue). The color change can persist for several seconds to minutes, although the tagging process occurs within nanoseconds. The photochromic process is reversible, therefore the chemical is reusable. The use of photochromic chemicals requires two photon sources; typically a pulsed UV source (e.g. $\lambda = 351$ nm from an excimer laser) to induce the color change and a white light source to interrogate the tagged regions. With the development of water-soluble compounds, the use of this velocimetry approach is expanding. Applications of chemically modified water-soluble photochromic dyes have been reported by Douglas et al. (1991) and Yurechko and Ryazantsev (1991). The most significant drawback in using photochromic chemicals is that the image is produced by a change in absorbance, thereby requiring a measurement of the difference between incident and transmitted light. Emitted light (against a black background) is more easily and accurately detected than transmitted light; consequently, images based on luminescence are better suited to MTV applications.

Caged fluorescein and similar compounds have recently become available, and their use was first introduced by Lempert et al. (1995) and Harris et al. (1996). In this compound

a chemical group is attached to fluorescein in order to render it non-fluorescent. The caging group is removed upon absorption of UV photons ($\lambda = 350$ nm), thereby creating regular fluorescein which fluoresces with a very high quantum efficiency. Here the long-lifetime tracer is the uncaged fluorescein, which persists for a very long time and can be interrogated at the time of interest through its luminescence upon re-irradiation. Two sources of photons are therefore needed, one to break the cage and the other to excite fluorescence. Two aspects of the current design of caged fluorescein require special attention when designing an experiment: The cage-breaking process is irreversible, so each caged molecule can be tagged only once. The cage-breaking process is not rapid, occurring with a time constant on the order of a few milliseconds. The delay between laser tagging and the generation of enough fluorescein to obtain an image with sufficient signal/noise dictates the fastest flow speeds that can be accommodated. In this paper we present a technique for overcoming this problem; see Sect. 3.3.

Although the emphasis of this paper is on liquid-phase flows, it is worth noting some of the gas-phase developments. The use of excited-state oxygen fluorescence was pioneered by Miles et al. (1987, 1989, 1993). The phosphorescence of biacetyl has been utilized by Hilbert and Falco (1991) and Stier et al. (1995), but its use is limited to oxygen-free environments due to the quenching effects of oxygen. The review by Falco and Nocera (1993) discusses many of the efforts known at that time; the review by Koochesfahani et al. (1996) provides a more recent summary of the developments in molecular tagging velocimetry.

The purpose of this paper is to describe the development and application of a new class of recently engineered water-soluble compounds suitable for molecular tagging diagnostics. Early utilization of these compounds has been presented by Koochesfahani et al. (1993), Hill and Klewicki (1994), Stier (1994), Gendrich et al. (1994), Cohn et al. (1995), and others. This paper provides information on the new phosphorescent complexes and discusses their properties relevant to the optimal design of an MTV implementation. Improvements in the optical and image acquisition implementations are reported. Our development of a more flexible data processing approach (Gendrich and Koochesfahani 1996) has increased the accuracy of the velocity estimates, and it also permits us to extend this velocimetry technique to cases where uniform seeding is not required. Novel applications for studying the Lagrangian evolution of mixing interfaces and making combined passive scalar/velocity measurements are demonstrated in this paper.

2
Phosphorescent supramolecules

When a phosphorescent compound is used for molecular tagging, excitation by photons produces a long-lived excited state which is interrogated through its phosphorescence emission as the molecule radiatively returns to its ground state. The long-lifetime tracer is the excited-state molecule itself. In this case only one source of photons is needed; the tagging process occurs during the laser pulse (a few nanoseconds in our case); and the excitation/emission process is reversible, which means the chemicals are reusable. The difficulty is that the long-lived excited states suffer from O_2 and H_2O quenching, and as a result suitable molecular complexes have not been available until recently.

New findings by Nocera and his group (Ponce et al. 1993; Mortellaro and Nocera 1996; Hartmann et al. 1996) show that supramolecules may be designed to exhibit long-lived phosphoresence which is not quenched. A successful design by Ponce et al. (1993) indicates that the quenching of a lumophore can be prevented and the phosphorescence emission recovered by mixing certain alcohols (indicated collectively by "ROH") with an aqueous solution of a cyclodextrin (CD) cup that contains the lumophore (Fig. 1). Cyclodextrins are molecules constructed from sugars connected in a head-to-tail arrangement. The molecule is cup-shaped and its size is determined by the number of sugars in the structure. The CD used in our application is Gß-CD, which is constructed of 7 glucose subunits, with one additional glucose bonded to the rim of the cup to improve its solubility in water. The resulting outer cup dimension is 15.3 Å, and the inner cup cavity has a diameter of 7.8 Å. The size of the cavity is important for effective binding to the lumophore, in our case 1-bromonaphthalene (1-BrNp), which absorbs efficiently at $\lambda = 308$ nm. When an appropriate alcohol is added, a ternary complex (1-BrNp · Gß-CD · ROH) is formed, where the alcohol hydrogen bonds to the rim of the CD and acts as a lid for the cup, thereby shielding the 1-BrNp from oxygen. (For this particular supramolecule the phosphorescence is not significantly quenched by H_2O.) The phosphorescence enhancement can be very large, approaching 10^4–10^5, depending on the fit of the alcohol lid to the CD cup; see Fig. 1.

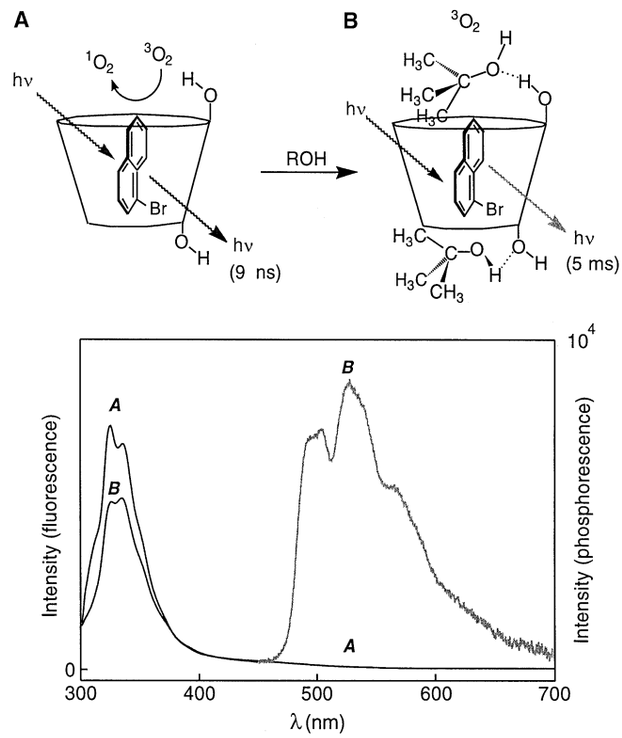

Fig. 1. Emission for 1-BrNp in CDs. *A* Only blue fluorescence is exhibited in the absence of an appropriate alcohol (ROH); *B* A bright green phosphorescence plus the initial fluorescence is seen upon the addition of *tert*-butanol, which prevents the quenching of the 1-BrNp phosphorescence by O_2

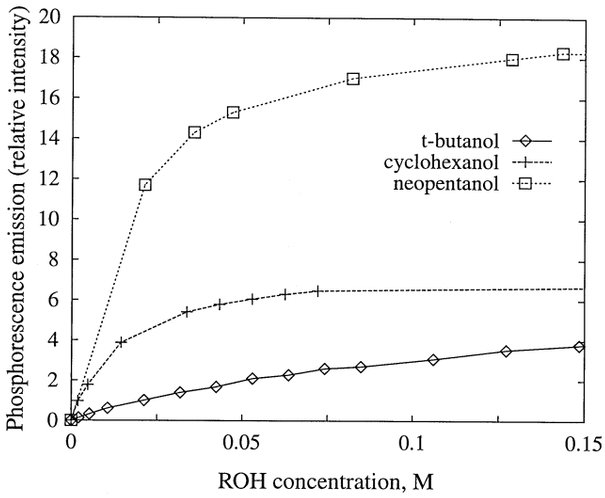

Fig. 2. Total phosphorescence emission from 1-BrNp · Gß-CD · ROH for three different types of alcohol at fixed concentrations of 1-BrNp and Gß-CD

A wide variety of alcohols may be used to cap the CD cup, see Ponce et al. (1993) and Hartmann et al. (1996). The choices of the alcohol and its concentration strongly influence the phosphorescence lifetime and intensity. Figure 2 shows the dependence of total phosphorescence emission on concentration for three different types of alcohol, *tert*-butanol (*t*-buOH), cyclohexanol (cycOH), and neopentanol (neopOH). The lifetimes for *t*-buOH and cycOH have been measured to be about 5 and 4 ms, respectively, for the alcohol- and CD-concentration independent ranges.

One disadvantage of the phosphorescent supramolecules described here is their lower quantum efficiency ($\phi_e = 0.035$) compared to that of uncaged fluorescein ($\phi_e = 0.90$). This is offset, however, by the advantages of reusability, the need for only one photon source, and a lower cost (estimated to be between 5 and 100 times less, depending on whether a CW or pulsed laser source is used to interrogate the uncaged fluorescein). Regardless of these comparisons, very low speed flows necessitating extremely long delay times between tagging and interrogation are best investigated using caged fluorescein or photochromic dyes.

The fact that mixing three components is required to produce the phosphorescent complex described here allows us to implement other applications beyond the traditional one of just velocimetry. These other applications include molecularly tagging a passive scalar mixing region and monitoring its Lagrangian evolution and molecularly tagging a chemical reaction interface between two streams and observing its Lagrangian evolution.

2.1
Optimization and preparation of the 1-BrNp · Gß-CD · ROH complex

When using phosphorescent molecules for molecular tagging purposes, the images acquired at a prescribed time delay Δt after tagging are always less intense than those acquired right after tagging due to the exponential decay of the luminescence. To obtain the highest possible image signal-to-noise, the chemical composition must be selected to yield the highest intensity for the selected Δt. For this reason an excess of immiscible 1-BrNp is always present to maintain a saturated solution of the lumophore (typically a molar concentration of order 10^{-5} M). The choice of an alcohol and its concentration is based on data such as that in Fig. 2. It can be seen that neopOH at 0.15 M is expected to produce the highest intensity, but unfortunately the use of neopOH in large-scale experiments is cost-prohibitive. The complex made using cyclohexanol, the next best choice, yields 90% of its maximum intensity at an alcohol concentration of 0.05 M. These are the alcohol and concentration that are used throughout this work. The selection of the CD concentration is driven by the fact that an increase in its concentration results in more phosphorescence but a reduced laser beam penetration length, owing to the increased absorption of the phosphorescent complex. For a typical working distance of 30–40 cm in our applications, we have found the optimal CD concentration to be 2×10^{-4} M or less, depending on the actual laser path length. For the mixture composition described here, the laser beam attenuation was measured to be approximately 0.01 cm^{-1}, and the corresponding lifetime is $\tau \cong 3.7$ ms.

In using these phosphorescent complexes, it is useful to recall that the luminecence lifetime refers to the time when the emission has decayed to 37% (e^{-1}) of its initial intensity. The actual usable delay time between laser tagging and interrogation can be considerably longer and is dictated by the type of detection used. We have measured flows using delays of up to 30 ms by employing image-intensified cameras.

3
Experimental setup and data reduction methods

Our applications of phosphorescent supramolecules are demonstrated here in the flow field of a vortex ring impinging on a flat wall at normal incidence. In this section we describe the experimental facility in which the vortex rings are generated, the laser and optics used to tag the flow, the arrangement of cameras and data acquisition systems for interrogating the tagged regions, and the processing technique by which velocity fields are extracted.

3.1
Flow facility

Figure 3 depicts a schematic of the flow facility. The vortex ring generator is a gravity-driven system through which a small slug of fluid is ejected into a reservoir from a vertical tube during a short interval controlled by a solenoid valve. For the flows discussed here, a 6 cm long slug of fluid was ejected during the 0.5 s opening of the solenoid valve. The ejected fluid originates only within the terminal straight portion of the generator and is not affected by the pipe bends or the valve upstream. The resulting vortex ring propagates downwards with a convection speed of about 5 cm/s, and its circulation is estimated to be $\Gamma = 52$ cm^2/s by integrating the vorticity field determined from velocity maps such as those shown in Fig. 11 (see Sect. 4). The corresponding Reynolds number is $\Gamma/\nu = 5200$. A flat solid wall is placed normal to the ring axis at a distance of 2.75 diameters away from the lip of the vortex generator.

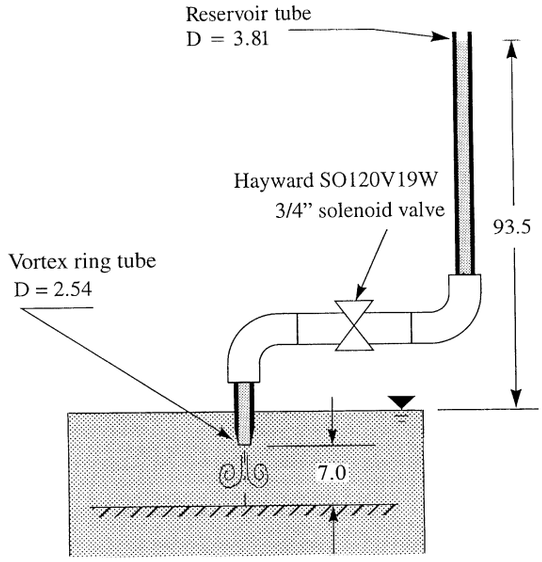

Fig. 3. Vortex ring experimental facility. Dimensions are in (cm) unless otherwise noted

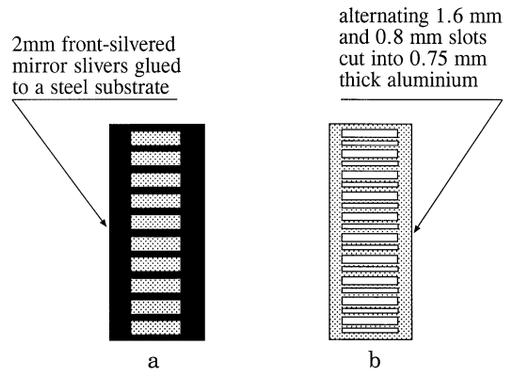

Fig. 4a, b. Optical devices to create patterned illumination. **a** A beam divider as developed by Falco and Chu (1987); **b** an example of one beam blocker configuration

3.2
Tagging methods and laser optical setup

Tagging the flow along single lines was originally used by Hummel and his group (e.g. Popovich and Hummel 1967; Ojha et al. 1989). Laser line tagging is still the only method used to date in the works utilizing caged fluorescein (Lempert et al. 1995; Harris et al. 1996) and excited-state oxygen fluorescence (Miles et al. 1987, 1989, 1993). The velocity is determined from the displacement of the tagged lines in much the same manner as using hydrogen bubble lines generated by a wire (see for example Lu and Smith 1985). It is very important to recognize that line tagging allows the measurement of only one component of velocity, that normal to the tagged line. In addition, the estimate of this velocity component has an inherent error associated with it (see Hill and Klewicki 1996; Koochesfahani et al. 1996).

In order to unambiguously measure two components of the velocity in a plane, the luminescence intensity field from a tagged region must have spatial gradients in two, preferably orthogonal, directions. For single-point velocimetry, this is easily achieved using a pair of crossing laser beams; a grid of intersecting laser lines allows multi-point velocity measurements. Use of this tagging scheme was first suggested by D'Arco et al. (1982), and it was later improved upon and utilized by Falco and Chu (1987). In the approach of Falco and Chu (1987), which is still commonly used, the main laser beam is split into multiple lines by an array of small mirrors. We have developed a much simpler device for this purpose; an aluminum plate with a series of thin slots blocks a portion of the incident beam, thereby generating multiple laser lines. Figure 4 contrasts these two different approaches. Clearly, the beam blockers allow a smaller fraction of the total laser energy to be used for tagging purposes, however beam blockers with arbitrary slot patterns can be designed and constructed much more quickly and inexpensively than a similar mirror array. The advantages become clearer when the width and the number of laser lines have to be optimized for a particular experiment, or when beams of non-uniform thickness are needed to simplify the spatial correlation procedure described in Sect. 3.4. We note that with improved detection and processing methods, we have been able to obtain high quality data with beam blockers that transmit as little as 30% of the incident energy. It is anticipated that these crude beam splitting techniques will be improved upon in the future by holographic and binary optics.

The UV laser beam used in these experiments is produced by a Lambda Physik 220 iCC excimer laser filled with XeCl. This laser provides 20 ns pulses at a wavelength of 308 nm with a pulse energy between 50 and 200 mJ and repetition rates up to 200 Hz. In a typical arrangement, see Fig. 5, the main laser beam, which is initially a 3.8×1.3 cm rectangle, is passed through a pair of cylindrical lenses in order to increase the aspect ratio. The outgoing beam is split using a 50:50 beam splitter, and then each of the resultant beams passes through a beam blocker to generate the laser grid pattern. The depth Δz of the beams in the direction normal to the plane of the grid pattern is typically 250 μm, and the energy in each beam thus generated varies between 1 mJ and 2 mJ given an incoming main laser beam of 100 mJ. Spherical lenses are used as needed to control the spatial scaling of the entire grid pattern. The inset in Fig. 5 shows an example of a region tagged by a grid pattern generated in this manner using a beam blocker with nearly uniform slot width and spacing.

As will be seen later, laser grid tagging is only a special case of a more generalized approach to induce a spatially non-uniform luminescence intensity in a tagged region. For example, the non-uniform passive scalar concentration field typical of most turbulent flows can sometimes be used as a natural source of luminescence non-uniformity (see Sect. 4.2).

3.3
Detection

The common element among all previous studies is that a single detector is used; the initial tagging pattern is recorded once, usually at the beginning of the experiment, and then the delayed images are acquired. The implicit assumption in this

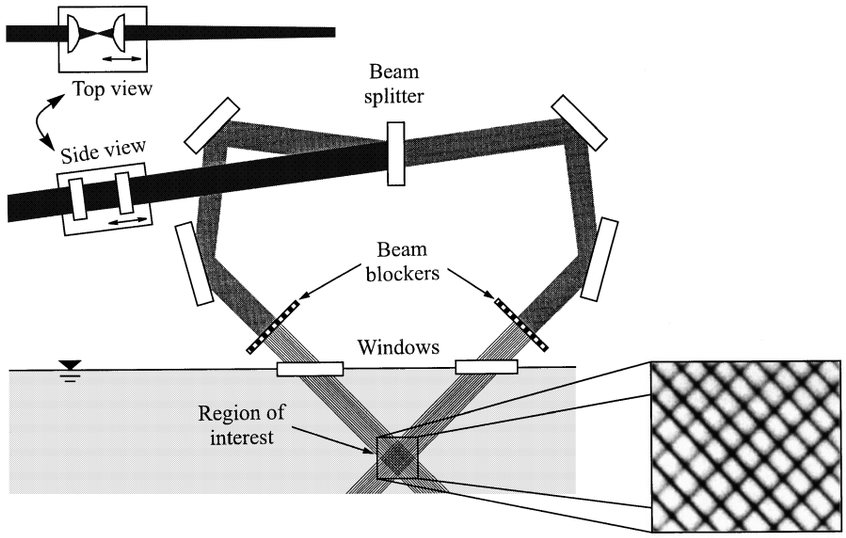

Fig. 5. Typical laser optics arrangement. Inset shows a region tagged using beam blockers with uniform slot width and spacing. Both top- and side-views are shown of the cylindrical lens arrangement which increases the beam aspect ratio

approach is that the initial tagging pattern remains spatially invariant throughout the experiment; therefore, any variations in the initial pattern (e.g. due to laser beam pointing instability, vibration of the optics, etc.) will be misinterpreted as flow velocity fluctuations.

In order to minimize the potential problem just noted, and to create a more flexible system to accommodate cases where no assumption can be made *a priori* about the intensity field in a tagged region, we have implemented a two-detector imaging system. The experimental arrangement, shown in Fig. 6, involves a link beween the laser and the two image detectors through a digital delay generator (Stanford Research Systems DG-535). Immediately after the laser fires, the first detector records an earlier image of the tagged flow, and after a prescribed time delay Δt, the second detector records a later image. The selection of time delay between tagging and interrogation is dictated by several factors. A larger delay will produce larger displacements and therefore a higher dynamic range in the velocity measurement. However, an increase in Δt leads to a degraded S/N in the delayed image, and it can also produce large distortions due to the strain rate and vorticity fields, which limits the effectiveness of the correlation procedure in estimating the displacement field (see Sect. 3.4). For the typical values of Δt in our experiments, we obtain maximum displacements in the range of 10–15 pixels corresponding to a real displacement in the range of 0.4–1.5 mm, depending on the image ratio.

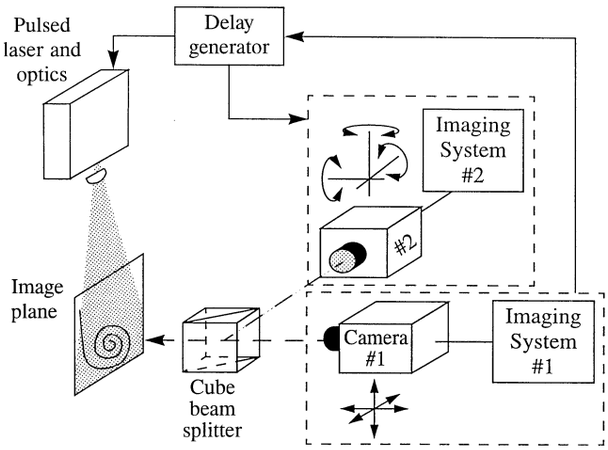

Fig. 6. 2-camera optical arrangement. Both cameras view the same image plane through the cube beam splitter. Synchronization between the two cameras and the laser is provided by a digital delay generator

In the arrangement shown in Fig. 6, the two detectors view the same region of interest in the flow through a cube beam splitter. The alignment of the two cameras relative to each other is adjusted with a 3-axis translation stage on one camera and a 3-axis rotation stage on the other. Using a reference target, the two cameras are aligned to one pixel, after which the two components of the actual displacement field $D_x(x, y)$ and $D_y(x, y)$ are determined to sub-pixel accuracy using the processing approach described in Sect. 3.4. This apparent displacement at zero velocity, which is very difficult to make identically zero uniformly over the entire sensor surface, is taken into account when computing the actual displacement due to the flow for each image pair. The alignment is verified to be the same before and after each run. The images are digitized to 8 bits into a 512×512 pixel array by two Trapix-Plus image acquisition/processing systems (Recognition Concepts, Inc.) and transferred onto a high capacity (10 GB) disk array in real time.

The data shown in this paper are acquired using the setup shown in Fig. 6 in conjunction with a variety of CCD detectors (electronically-shuttered frame transfer cameras or gated image-intensified cameras), depending on the optical/imaging requirements unique to the particular field of view. Typically for fields of view larger than about 3 cm, non-intensified Pulnix frame transfer cameras (TM-9701) are used along with Nikon 50 mm *f*/1.2 lenses. For smaller fields of view, Xybion gated image-intensified detectors (ISG-350-GW3) are utilized in conjunction with Nikon 105 mm *f*/2.8 Micro-Nikkor lenses.

Our two-detector approach clearly brings additional complexity to the experimental setup, such as having to align two

detectors and record the data using two synchronized image acquisition systems. However, it does resolve some major issues in the applications of this technique as detailed earlier. One additional advantage of this approach is in the use of caged fluorescein for high speed flow studies. The previously mentioned delay between tagging and uncaging of the fluorescein (see Sect. 2.2) becomes unimportant if the tagged regions are interrogated *twice* after enough uncaged fluorescein is available to produce images with adequate signal-to-noise.

It should be noted that it is possible to use a single-detector, dual-frame recording technique, such as that used in current Digital Particle Image Velocimetry (DPIV) systems, to record the two images of the tagged regions for MTV. The required detector capabilities are quite different, however. In DPIV, two different laser pulses are placed at the desired times, Δt apart, on two consecutive frames. In MTV, by contrast, only one laser pulse is involved, the one used to tag the flow; detection (not illumination) is required at two different times. This can be done if the image sensor has the capability for asynchronous shuttering with variable duration at arbitrary times during a frame. Some of the newer frame transfer cameras have this capability; a gated image-intensified camera can also accomplish the same task. Using this approach, the advantages of a single detector and image acquisition system are offset by a factor of two reduction in velocity data rate and the reduced ability to optimize a single detector's output for two images of different intensities.

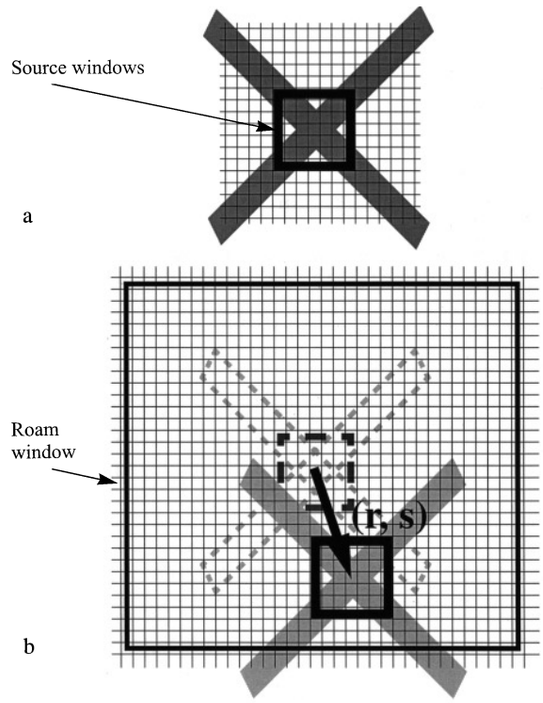

Fig. 7a, b. Spatial correlation technique schematic. **a** Tagged region at time $t = t_1$; **b** correlation of the source window with one portion of the roam window at time $t_2 = t_1 + \Delta t$; dashed lines indicate the original location of the region

3.4 Processing

The traditional method for finding the displacement of tagged lines or grids has been to locate the center of each line using various techniques. Most of the recent techniques use the best fit of the line's cross-section to an assumed laser line profile, for example, a Gaussian intensity distribution. The performance of this method will suffer when the intensity distribution of the tagged regions cannot be assumed in advance, for example, due to non-uniform mixtures, difficulties associated with laser beam transmission through a flowing medium, bleaching effects, etc.

We have taken a different approach in an attempt to implement a generalized scheme that is independent of the specific intensity distribution within a tagged region and which can accommodate arbitrary tagging patterns including those due to non-uniform scalar mixing fields. The displacement of the tagged regions is determined using a direct digital spatial correlation technique. The details of this approach and its performance can be found in Gendrich and Koochesfahani (1996); a brief description is given below.

A small window, referred to as the source window, is selected from a tagged region in the earlier image, and it is spatially correlated with a larger roam window in the second image; see Fig. 7. We calculate the spatial correlation coefficient $R(r, s)$ between the intensity field I_1 of the source window and $I_2(r, s)$ from the roam window as a function of the pixel displacement (r, s) between them:

$$R(r,s) = \frac{\overline{I_1 \cdot I_2} - \bar{I}_1 \cdot \bar{I}_2}{\sigma_{I_1} \cdot \sigma_{I_2}}$$

In this expression the overbar refers to the expected value, and σ denotes the standard deviation; with this definition, $-1 \leqslant R \leqslant +1$. Sub-pixel accuracy is obtained by locating the maximum in the fit of a 9×9 pixel region about the peak in $R(r, s)$ to a two-dimensional 7th-order polynomial. The computed displacement vector $(\Delta x, \Delta y)$ is corrected by subtracting the apparent camera displacement for zero velocity, $D_x(x, y)$ and $D_y(x, y)$, at the center of the source window; see Sect. 3.3 above. The spatial average of the velocity within the source window is then estimated according to $[u, v] = [(\Delta x - D_x)/\Delta t, (\Delta y - D_y)/\Delta t]$.

The example provided in Fig. 8 illustrates a region in an actual experiment tagged by a laser grid, the tagged region at a later time, and the corresponding spatial correlation coefficient field for one of the grid crossings. A single well-defined correlation peak occurs at the location corresponding to the displacement of the tagged region by the flow, and the displacement peak can be located to sub-pixel accuracy using the polynomial fit described above. Based on both experiments and an extensive statistical study on the performance of this correlation approach, we have found that we can typically measure the displacement of the tagged regions with a 95% confidence limit of ± 0.1 pixel (i.e. 95% of the displacement measurements are accurate to better than 0.1 pixel). This corresponds to an rms accuracy of ± 0.05 pixel, assuming a Gaussian distribution for error.

A similar procedure has been applied to process DPIV image pairs; see for example Fincham and Spedding (1995) and Roesgen and Totaro (1995). The correlation procedure

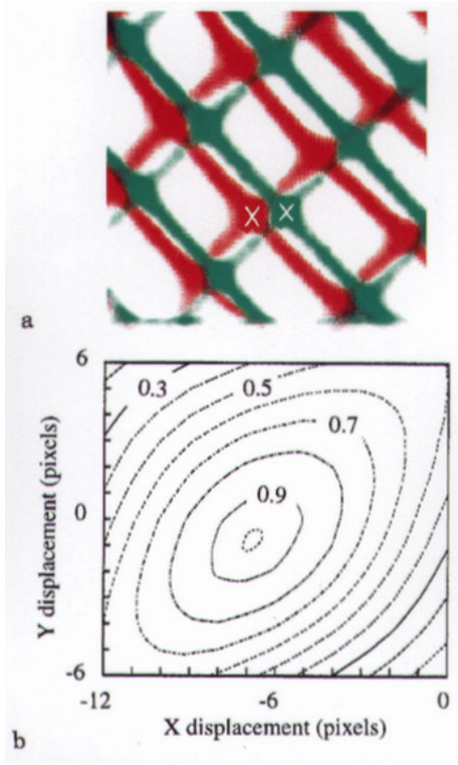

Fig. 8a, b. Experimental MTV grid. **a** Green lines are the grid at $t = 0$; red lines are the grid after a 6 ms delay; **b** correlation coefficient contours for the indicated intersection in **a**

described here is a first order method for estimating a linear displacement vector; it can be extended to accommodate the higher order derivatives.

4
Results

This section provides three different applications of the phosphorescent supramolecule presented in this paper. The flow visualization in Fig. 9 serves to acquaint the reader with the general characteristics of the test flow field. These images were obtained using two-color LIF, where the vortex ring and boundary layer fluids were labeled by green and red emitting laser dyes, respectively. The indicated time index is relative to the opening of the solenoid valve of the vortex generator. As the primary vortex ring approaches the wall (Fig. 9a), the unsteady adverse pressure gradient on the wall results in boundary layer separation and the formation of a secondary vortex of opposite sign to that of the primary (Fig. 9b). In this case as the primary and secondary vortices interact (Fig. 9c and d), a tertiary vortex is formed (Fig. 9d), and later in time the secondary vortex ring moves quickly away from the wall (Fig. 9e).

4.1
Homogeneous mixtures for kinematics

When only velocity information and other kinematics data such as strain rate and vorticity are required, the (1-BrNp · Gß-CD · cycOH) complex can be premixed in the entire flow

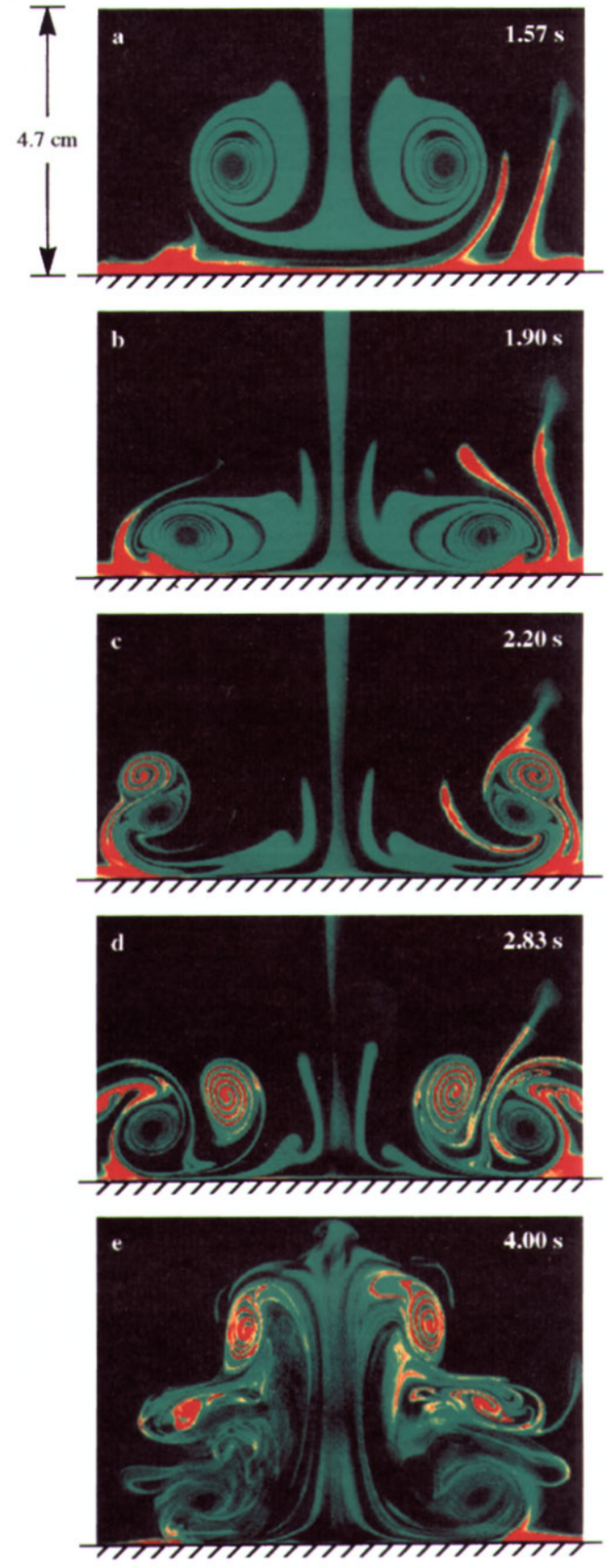

Fig. 9. Two-color LIF image sequence showing the development of the vortex ring/wall interaction. Times are relative to the opening of the solenoid valve (see Fig. 3)

facility. An example of tagging by a laser grid is shown in Fig. 10 for the flow field illustrated in Fig. 9a. The core of the vortex is approximately 2 cm above the wall. The rotation of the tagged region near the core is apparent in the delayed image. The time delay in this example was selected to produce a maximum flow displacement of 14 pixels (about 1.5 mm) while limiting the strain- and vorticity-induced distortions which could adversely affect the estimate of the linear displacement vector based on the correlation procedure.

The spatial distribution of the velocity field determined from the image pair of Fig. 10 is shown in Fig. 11. The data in this figure are raw, and bad vectors have not been removed. The primary vortex core is well captured. The time-series for the two velocity components (u, v) at a grid intersection on the axis of symmetry of the vortex ring are shown in Fig. 12. The data shown are again raw and have not been filtered or smoothed. Note that v-component remains near zero as expected for a point on the axis of symmetry; the rms fluctuation in the data is 0.051 cm/s (0.041 pixel) and, as expected, 95% of the v data fall within ± 0.1 pixel (or ± 0.125 cm/s) of zero.

While shorter time delays are desired for mapping the velocity field, longer time delays provide more direct information on the Lagrangian evolution of the flow under the influence of the strain rate and vorticity fields. An image pair highlighting this aspect is given in Fig. 13 at an instant in time close to that of Fig. 9b. The region near the wall shows the flow kinematics in the vicinity (both in time and space) of the boundary layer separation; the significant v velocity component of the separating boundary layer near the wall is readily apparent.

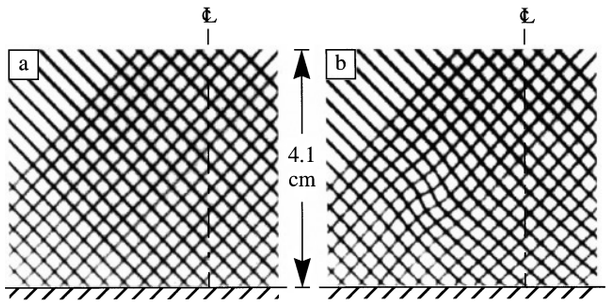

Fig. 10a, b. MTV grid for velocimetry. **a** 1 μs after laser pulse; **b** distorted grid 8 ms later. The vortex ring axis of symmetry is indicated by the dashed lines

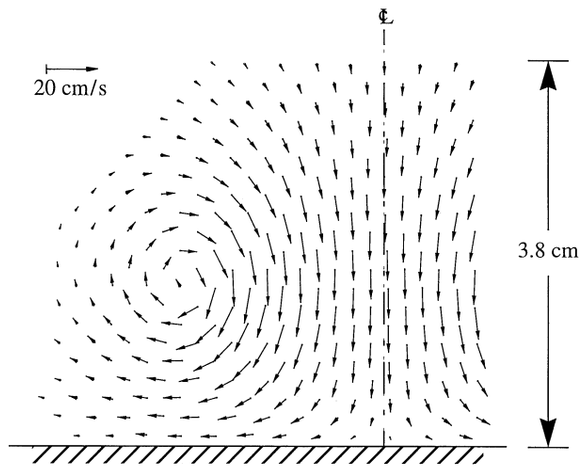

Fig. 11. Velocity vector field derived from the image pair in Fig. 10

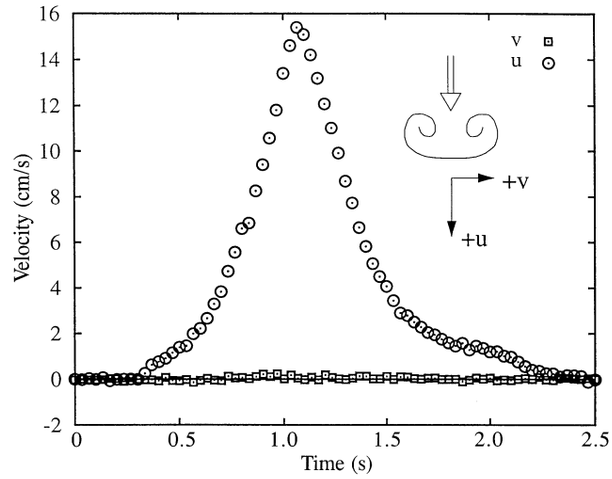

Fig. 12. Time evolution of the u- and v-velocity components near the center of a passing vortex ring

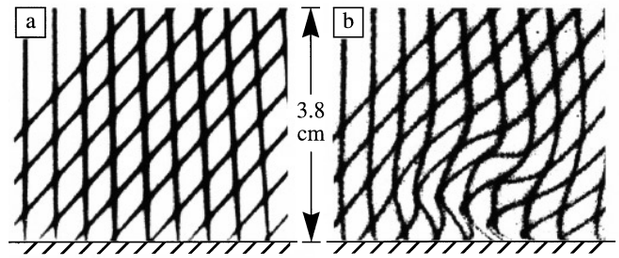

Fig. 13. Image pair with long time delay ($\Delta t = 17$ ms) showing the Lagrangian evolution of the tagged regions near flow separation

4.2
Passive scalar mixing and kinematics

For situations where information on passive scalar mixing and kinematics is desired, the alcohol, CD, and lumophore can be premixed in one stream, while the other mixing stream contains the alcohol and lumophore solution (i.e. the same solution as the first stream minus the CD). The Lagrangian evolution of the scalar mixing field is then monitored over the luminescence lifetime. An example of this implementation, where the vortex ring's fluid is premixed with all three elements of the phosphorescent complex, is shown in Fig. 14 for the flow field illustrated in Fig. 9a. The UV laser is arranged to illuminate a series of parallel "bands" in the flow. Figure 14a shows the superposition of the molecularly-tagged patches at

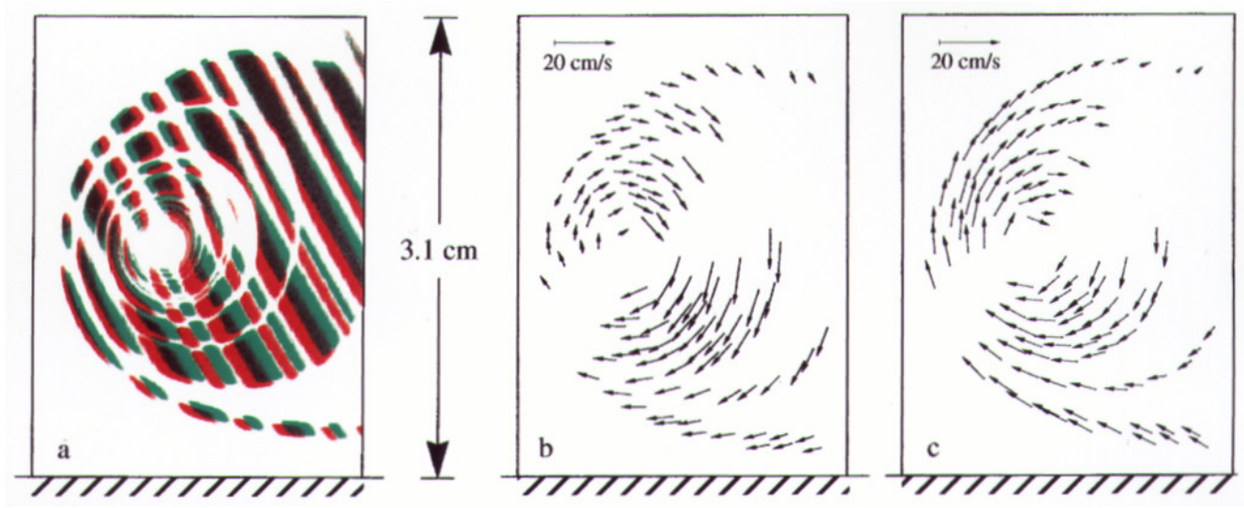

Fig. 14a–c. Lagrangian evolution of molecularly tagged fluid patches in a vortex ring. **a** Tagged patches at two different times; the green patches are 1 μs after laser tagging, and the red patches are 9 ms later; **b** velocity vectors derived from correlating the corners in **a**; **c** velocity vector with the vortex ring's core velocity subtracted

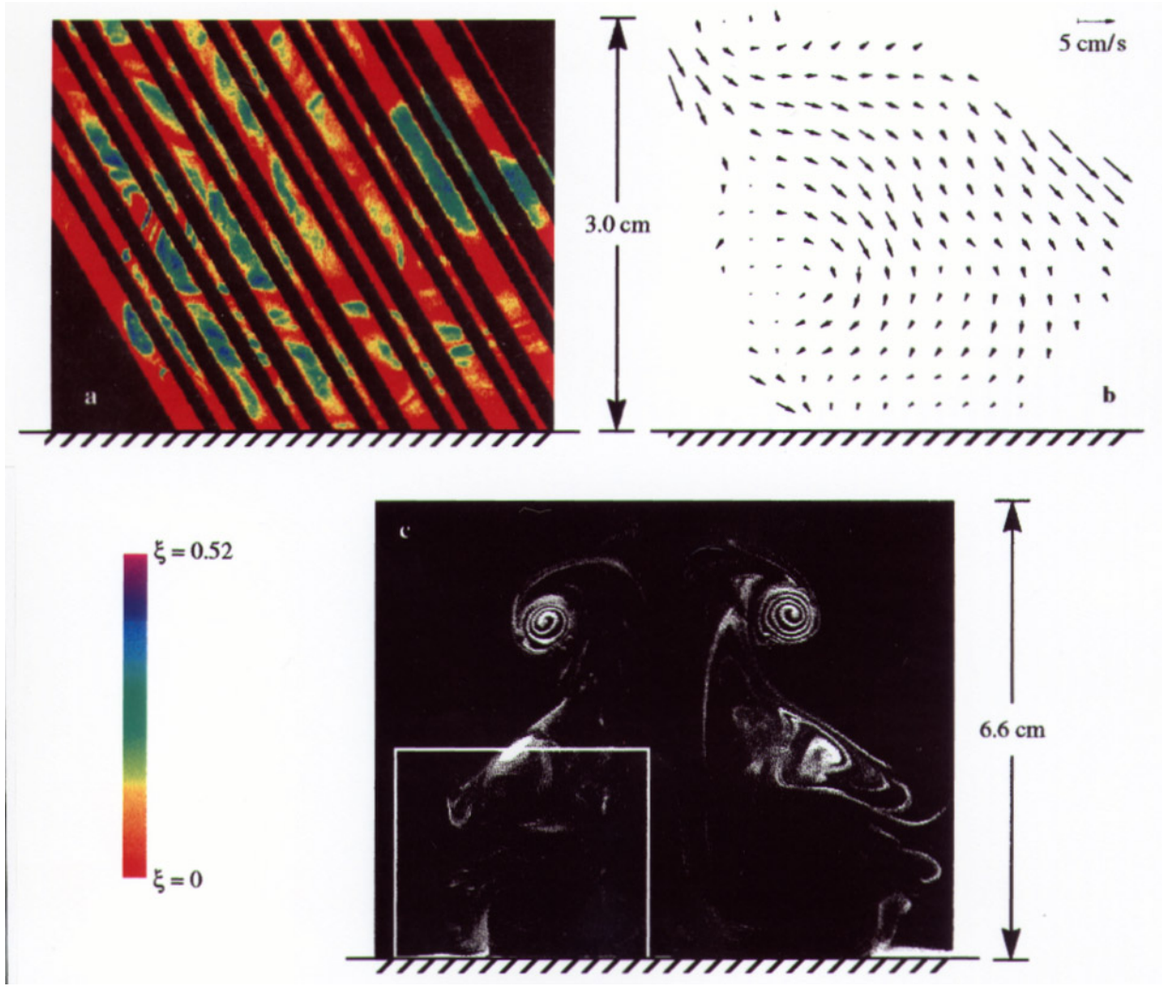

Fig. 16. a Passive scalar concentration field derived from an image 1 μs after laser tagging; **b** velocity field determined using **a** and the corresponding delayed image ($\Delta t = 19$ ms, not shown here); **c** LIF visualization of the gross flow features at this instant in time ($t = 4.33$ s). The highlighted box indicates the region shown in **a** and **b**

two different times. The flexibility of the correlation approach for extracting displacement information now becomes apparent as the velocity vectors at the corners of the patches are determined by this technique and displayed in Fig. 14b. The velocity field in the reference frame attached to the vortex core is indicated in Fig. 14c. The vortex core convection speed was determined from an examination of the flow visualization time series and confirmed by the movement of the location of the peak vorticity measured using MTV.

For the data just described, the time delay was relatively short. As discussed earlier for the premixed case, longer time delays provide more direct information on the Lagrangian evolution of the tagged patches. Figure 15, which corresponds to the instant depicted in Fig. 9c, offers many good examples of large deformations in marked fluid patches as they convect. The four tagged patches highlighted in the enlarged views of Fig. 15c and d reveal some of the interesting kinematics made visible by the molecular tagging approach. Note the compression along the vortex pair axis of the two small patches near the leading edge, and their expansion normal to that axis due to the high strain rate in that area. The third small patch near the rear of the vortex pair experiences the opposite effect, an expansion along the axis and a compression normal to it. The large tagged region shows large deformations as a result of the widely varying underlying strain and vorticity fields.

Even though the examples discussed so far have a rather simple concentration field (uniform within the tagged patches), they highlight the potential of a molecular tagging approach to simultaneously measure the concentration field (from the first image) and the velocity field (using image pairs) in more complex and turbulent flows. Figure 16 demonstrates this capability, where the scalar field is nonuniform as a result of the mixing between the vortex ring and ambient fluids. A 3 cm region of the flow next to the wall is illuminated by parallel bands of laser light, and the resulting normalized concentration field ξ is shown in Fig. 16a. The range of ξ is selected such that the value $\xi = 0$ corresponds to the ambient fluid and $\xi = 1$ is the pure vortex ring fluid. The areas in the flow which were not illuminated are colored black, and the illumination non-uniformity has been accounted for. The corresponding velocity field is obtained using the image in Fig. 16a and its delayed counterpart (not shown here; $\Delta t = 19$ ms due to the slow flow speeds) and correlating small regions within each illuminated band. The additional spatial non-uniformity of the luminescence field within these regions due to the non-uniform scalar field does not adversely affect the correlation procedure. In fact, this feature allows velocity vectors to be determined for different regions along the illuminated bands, which would not have been possible with a uniform concentration field. The velocity field remapped onto a regular grid is shown in Fig. 16b. In order to facilitate the interpretation of this velocity field, we show in Fig. 16c an LIF visualization at this instant in time with the region of interest highlighted by a white box. It should be emphasized that this LIF image is intended to serve only as representative of the gross features of the flow. Although the data of Fig. 16a and c are different realizations of the same instant in time, the flow features and concentration field are not highly repeatable at this late stage of the flow evolution.

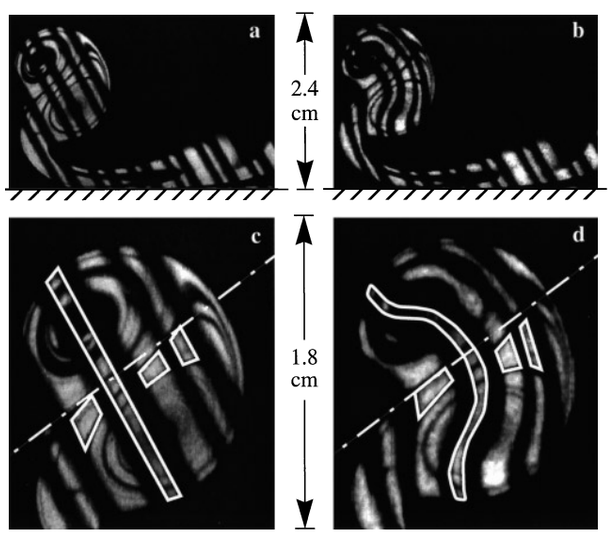

Fig. 15a–d. Lagrangian evolution of tagged patches of the scalar mixing field. **a** 1 μs after laser tagging; **b** 19 ms later; **c** and **d** are enlarged views of **a** and **b** respectively

As noted in Sect. 3.2, a luminescence intensity gradient in two directions is required to determine the two components of the velocity vector. Tagging by a laser grid is a simple way to accomplish this. The use of a grid pattern can be relaxed as a result of the naturally occurring intensity variation due to a non-uniform concentration field; Figs. 14 and 16 provide two examples of this. The spatially non-uniform scalar concentration field typical of most turbulent flows can, in some cases, be used as the sole source of the required luminescence intensity variation. It is understood that this implies the presence of sufficient intensity gradients within each source window used for the correlation procedure. In situations where this can be accomplished, a much simpler optical arrangement with a laser sheet can replace the somewhat more involved technique of "writing" a prescribed laser pattern into the flow. An example involving the vortex ring of a starting turbulent jet is given in Gendrich and Koochesfahani (1996).

4.3
Reaction interface kinematics

When all three components, 1-BrNp, Gß-CD and cycOH, are molecularly mixed, the phosphorescence complex is immediately activated. Therefore the proper placement of these components in mixing streams allows chemically reacting regions to become luminescent. As before, the Lagrangian evolution of these regions can be monitored over the luminescence lifetime of the complex.

Figure 17 is the chemically reacting counterpart of Fig. 9. In this experimental setup the vortex ring fluid is premixed with the CD and cycOH solution, whereas the ambient fluid contains the lumophore and cycOH. Sodium sulfate is added to the ambient fluid to match the density between the two streams. The images in Fig. 17, recorded immediately after illumination by a uniform laser sheet, show only those regions in the flow where the three components of the phosphorescent complex have mixed at the molecular level.

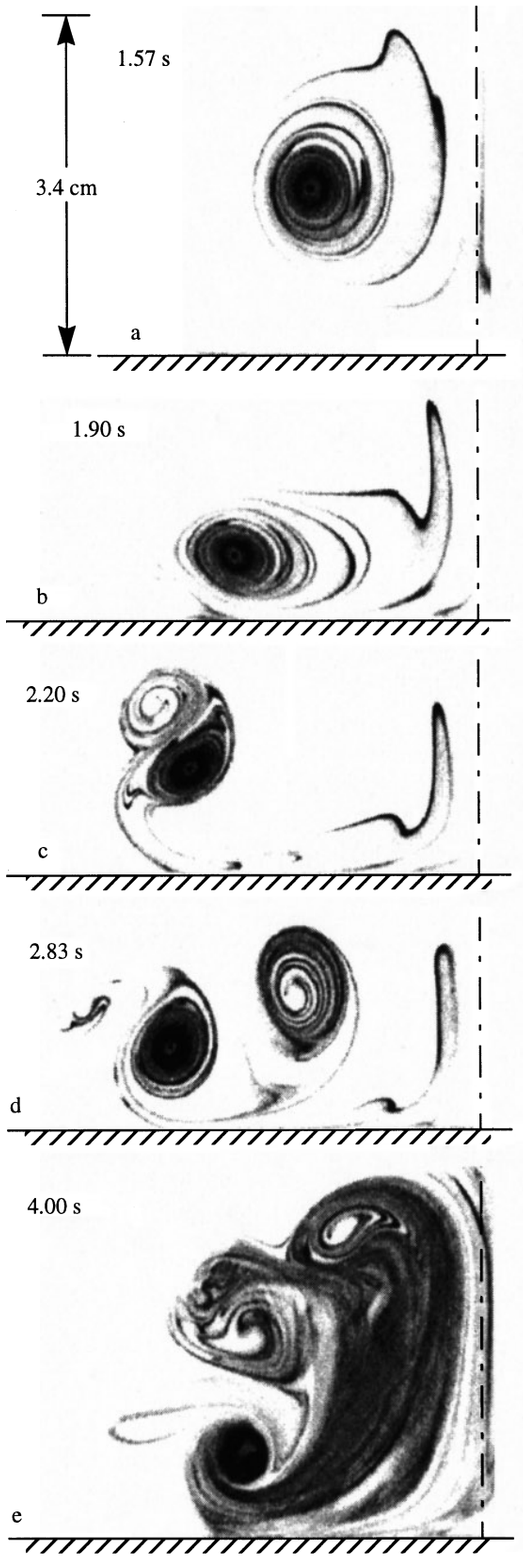

Fig. 17a–e. Chemical reaction interfaces tagged by a laser sheet

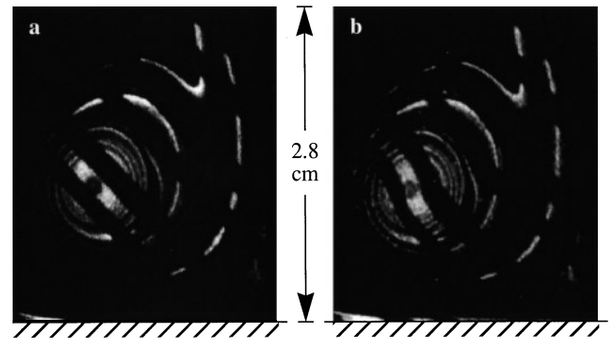

Fig. 18. Image pair with long time delay ($\Delta t = 12$ ms) showing the Lagrangian evolution of chemically reacting interfaces

A non-uniform illumination pattern makes it easier to identify smaller regions in the fluid and track their time evolution. Figure 18 was illuminated by parallel bands of the laser in the same manner as Figs 14–16. The displacement and rotation of the reacting interfaces, particularly in the vortex core, are visible. Data such as those shown here have also been used to determine velocity fields (not shown here) using the correlation procedure.

5 Conclusions

The development and applications of a new class of water-soluble compounds suitable for molecular tagging diagnostics are described. These compounds are based on complexes formed by mixing a lumophore with cyclodextrin and an appropriate alcohol. The CD acts as a "cup" and the alcohol as the "lid" to shield the lumophore from the quenching effects of oxygen and water. Using 1-BrNp as the lumophore, cyclohexanol is determined to be the most suitable overall among the alcohols for which data are currently available. Information is provided to allow the design of experiments based on these complexes.

Implementation of a two-detector system is described which, in combination with a spatial correlation technique for determining velocities (Gendrich and Koochesfahani, 1996), relaxes the requirement that the initial tagging pattern be known *a priori*, eliminates errors in velocity estimates caused by variations in the pattern during an experiment, and makes it possible to study flows with non-uniform mixtures. This detection and analysis combination also solves one of the problems associated with using caged fluorescein to study high-speed flows.

Applications for molecular tagging velocimetry (MTV) are provided using a less complex method of generating grid patterns. Beam blockers provide a more flexible, less expensive alternative to mirror arrays in cases when sufficient beam energy is available. Besides the traditional implementation of velocimetry, novel applications for studying the Lagrangian evolution of mixing interfaces (both reacting and non-reacting) and obtaining combined passive scalar/velocity measurements are also demonstrated in this paper.

References

Chu CC; Liao YY (1992) A quantitative study of the flow around an impulsively started circular cylinder. Exp Fluids 13: 137–146

Chu CC; Wang CT; Hsieh CH (1993) An experimental investigation of vortex motions near surfaces. Phys Fluids 5: 662–676

Cohn RK; Gendrich CP; MacKinnon CG; Koochesfahani MM (1995) Crossflow velocity measurements in a wake flow. Bull Am Phys Soc 40: 1962

D'Arco A; Charmet JC; Cloitre M (1982) Nouvelle technique de marquage d'écoulement par utilisation de molécules photochromes. Rev Phys Appl 17: 89–93

Douglas P; Enos RD; Azzopardi B; Hope CB (1991) Characterisation of a photochromic triarylmethane dye sulphite and its application to the visualisation of water flows. 7th Int. Topical Meeting on Photoacoustic and Photothermal Phenomena, The Netherlands, August 1991

Falco RE; Chu CC (1987) Measurement of two-dimensional fluid dynamic quantities using a photochromic grid tracing technique. SPIE 814: 706–710

Falco RE; Nocera DG (1993) Quantitative multipoint measurements and visualization of dense solid-liquid flows using laser induced photochemical anemometry (LIPA). In: ParticulateTwo-Phase Flow, (ed. MC Rocco), pp 59–126, London: Butterworth-Heinemann

Fincham AM; Spedding GR (1995) Velocity bandwidth discretization errors and peak-locking phenomena in DPIV measurements. Bull Am Phys Soc 40: 2000

Gendrich CP; Koochesfahani MM (1996) A spatial correlation technique for estimating velocity fields using Molecular Tagging Velocimetry (MTV). Exp Fluids 22: 67–77

Gendrich CP; Koochesfahani MM; Nocera DG (1994) Analysis of molecular tagging velocimetry images for obtaining simultaneous multi-point velocity vectors. Bull Am Phys Soc 39: 1980

Harris SR; Lempert WR; Hersh L; Burcham CL; Saville A; Miles RB; Gee K; Haughland RP (1996) Quantitative measurements on internal circulation in droplets using flow tagging velocimetry. AIAA J 34: 449–454

Hartmann WK; Gray MHB; Ponce A; Nocera DG (1996) Substrate induced phosphorescence from cyclodextrin lumophore host-guest complexes. Inorg Chim Acta 243: 239

Hilbert HS; Falco RE (1991) Measurements of flows during scavenging in a two-stroke engine. SAE Technical Paper 91067

Hill RB; Klewicki JC (1994) Developments and applications of laser induced photochemical anemometry. ASME Fluid Egr Div 191, Laser Anemometry – 1994: Advances and Applications: 209–216

Hill RB; Klewicki JC (1996) Data Reduction methods for flow tagging velocity measurements. Exp Fluids 20: 142–152

Koochesfahani MM; Cohn RK; Gendrich CP; Nocera DG (1996) Molecular tagging diagnostics for the study of kinematics and mixing in liquid phase flows. Proc 8th Int Symp on Applications of Laser Techniques to Fluid Mechanics, Lisbon, Portugal, 8–11 July, pp 1.2.1–1.2.12

Koochesfahani MM; Gendrich CP; Nocera DG (1993) A new technique for studying the Lagrangian evolution of mixing interfaces in water flows. Bull Am Phys Soc 38: 2287

Lempert WR; Magee K; Ronney P; Gee KR; Haughland RP (1995) Flow tagging velocimetry in incompressible flow using photo-activated nonintrusive tracking of molecular motion (PHANTOMM). Exp Fluids 18: 249–257

Lu LJ; Smith CR (1985) Image processing of hydrogen bubble visualization for determination of turbulence statistics and bursting characteristics. Exp Fluids 3: 349–356

Miles R; Cohen C; Conners J; Howard P; Huang S; Markovitz E; Russel G (1987) Velocity measurements by vibrational tagging and fluorescent probing of oxygen. Opt Let 12: 861–863

Miles RB; Connors JJ; Markovitz EC; Howard PJ; Roth GJ (1989) Instantaneous profiles and turbulence statistics of supersonic free shear layers by Raman excitation plus laser-induced electronic fluorescence (Relief) velocity tagging of oxygen. Exp Fluids 8: 17–24

Miles RB; Zhou D; Zhang B; Lempert WR; She ZS (1993) Fundamental turbulence measurements by Relief flow tagging. AIAA J 31: 447–452

Mortellaro MA; Nocera DG (1996) A turn-on for optical sensing. ChemTech 26: 17–23

Ojha M; Cobbold RSC; Johnston KW; Hummel R (1989) Pulsatile flow through constricted tubes: an experimental investigation using photochromic tracer methods. J Fluid Mech 203: 173–197

Ponce A; Wong PA; Way JJ; Nocera DG (1993) Intense phosphorescence triggered by alcohols upon formation of a cyclodextrin ternary complex. J Phys Chem 97: 11137

Popovich AT; Hummel RL (1967) A new method for non-disturbing turbulent flow measurement very close to a wall. Chem Eng Soc 22: 21–25

Roesgen T; Totaro R (1995) Two-dimensional on-line particle imaging velocimetry. Exp Fluids 19: 188

Stier B (1994) An investigation of fluid flow during the induction stroke of a water analog model of an IC engine using an innovative optical velocimetry concept – LIPA. PhD Thesis, Michigan State University, East Lansing, Michigan

Stier B; Koochesfahani MM; Nocera DG; Schock HJ (1995) Molecular tagging velocimetry in gas phase flow. Bull Am Phys Soc 40: 1962

Yurechko VN; Ryazantsev Yu S (1991) Fluid motion investigation by the photochromic flow visualization technique. Exp Thermal and Fluid Sci 4: 273–288